Chapter 10

Bioimpedance Technique for Point-of-Care Devices Relying on Disposable Label-Free Sensors – An Anemia Detection Case

Jaime Punter-Villagrasa, Joan Cid,
Jordi Colomer-Farrarons,
Ivón Rodríguez-Villarreal and Pere Ll. Miribel-Català

Additional information is available at the end of the chapter

http://dx.doi.org/10.5772/60843

Abstract

In this chapter, the development of a point-of-care device for bio-medical applications has been discussed. Our main objective is to research new electronic solutions for the detection, quantification, and monitoring of important biological agents in medical environments. The proposed systems and technologies rely on label-free disposable sensors, with portable electronics for user-friendly, low-cost solutions for medical disease diagnosis, monitoring, and treatment. In this chapter, we will focus on a specific point-of-care device for cellular analysis, applied to the case of anemia detection and monitoring. The methodology used for anemia monitoring is based on hematocrit measurement directly from whole blood samples by means of impedance analysis. The designed device is based on straightforward electronic standards for low power consumption and low-cost disposable sensor for low volume samples, resulting in a robust and low power consumption device for portable monitoring purposes of anemia. The device has been validated through different whole blood samples to prove the response, effectiveness, and robustness to detect anemia.

Keywords: Point of care, electronics, impedance analysis, whole blood, hematocrit

1. Introduction

The integration of medical and electronic technologies allows the development of biomedical devices able to diagnose and/or treat pathologies by detecting, quantifying, and monitoring cellular species in different conductive media. In this chapter, the main attention is focused on the development of instrumentation electronics and sensing systems as well as design protocols for point-of-care (PoC) devices for cellular detection and monitoring, relying on straightforward standards for economic, low power consumption, versatile, safe, and reliable devices.

Several studies have reported that cellular detection, quantification, and monitoring can be accurately monitored by means of its biological electrical impedance (BioZ) [1-10] in different environments, in vivo or ex vivo experiences. One example of such work is the paper presented by Pop et al. (2013) [2], where blood hematocrit (HCT) was continuously in vivo monitored in the human right atrium by a dedicated central venous catheter equipped with an impedance measuring device. Pradhan et al. (2012) [5] studied ex vivo the electrical properties of blood and its constituents using impedance spectroscopy (IS) and three-electrode sensors. Ramaswamy et al. (2013) [6] performed a blood coagulation test based on a custom microfluidic device and the electrical impedance detection of whole blood samples. Li et al. (2012) [8] monitored Legionella serogroups in clinical and environmental samples by means of IS. Dweik et al. (2012) [9] demonstrated the detection of E. coli where bacterial presence was rapidly detected by measuring the antibody-antigen bonding by impedance analysis between 100 Hz and 10 MHz. Also, in the work developed by Grossi et al. (2010) [10], the quantity of bacteria during a culture process was detected by impedance measured at 200 Hz sinusoidal with a 100 mV peak-to-peak signal. Furthermore, other studies have reported the detection of cell-derived microparticles [11] and insulin in blood serum [12] based on an IS technique.

1.1. Biological electrical impedance

Dilute cellular sample suspensions can be described as a network of electrical passive components. The BioZ, identical to the definition from the Ohm's law [13], is defined as the response of applying an electrical stimulus to a biological material through a sensing system and measuring its electrical response. The electrical response is frequency dependant, and depending on the samples under examination and the sensing system, there are different frequency working ranges where an appropriate electric response can be found, so a frequency sweep is needed to evaluate the electrical response of the whole designed system (biological sample along with the sensing system). There are different sensing electrodes topologies to be considered depending on the number of electrodes used. Typical cellular electrical model for dilute cell suspensions can be described as network of electrical components [14] (Figure 1).

Injected current can flow through external media (R_E resistance) or through the cell across the membrane ($R_M \| C_M$) and the intracellular medium (R_I resistance). Considering that R_M resistance is nearly negligible, a simplified model is considered.

http://dx.doi.org/10.5772/60843

$$Z_{CELL} = \frac{R_E\left(1 + j\omega C_M R_1\right)}{1 + j\omega C_M\left(R_1 + R_E\right)}$$

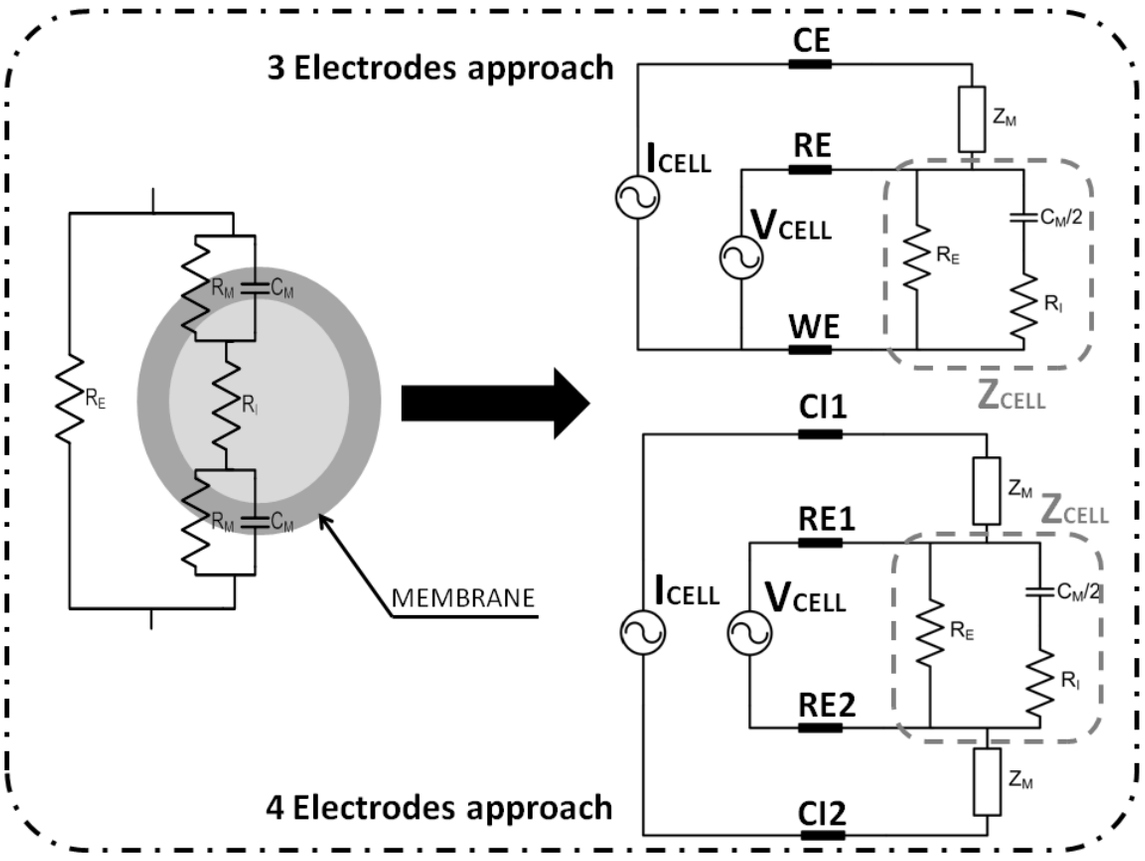

Figure 1. Cellular electrical model. Sensing system based on 3 electrodes and 4 electrodes approach.

A two-electrode topology is defined by the working electrode (WE), where the sample is placed and the electrical signal is applied, in addition to the auxiliary electrode (AE), which tracks the solution potential and supplies the current required for experience. This topology brings some kind of problematic behavior by the AE polarization effects causing a distortion of the applied electrical signal. The three-electrode configuration is defined as follows: the working electrode (WE), where the object is under investigation, the reference electrode (RE), which tracks the electric signal, and the counter or auxiliary electrode (CE), which supplies the required current. This topology avoids the distortion of the applied electrical signal.

Finally, the fourelectrode configuration avoids the measurement distortion due to the WE impedance polarization, as in the threeelectrode topology, the electric signal is directly applied where the single-ended voltage measurement signal is read. The fourelectrode topology is composed of two current-injection electrodes and two voltage-reading electrodes avoiding the electrode polarization distortion in impedance measurement due to a complete differential voltage measurement [15].

BioZ technique allows the use of different sensing topologies and systems, making possible the integration of such electrodes in a great variety of devices and environments, such as biosensors and microfluidic devices for increased functionality and performance. Moreover, the simplicity of the technique implementation makes it possible to accomplish the experience objectives with very simple sensing systems. Hernández et al. (2011) [4] obtained the electric impedance spectrum of human blood using reactive strips of the Bayer's portable glucometer.

The electronics involved in customized PoC devices are implemented as a front-end electronics depending on the sensing topology, and a back-end user interface for data processing and user interface. As a general standard, the whole PoC device can be described in a general outline as it is depicted in Figure 2.

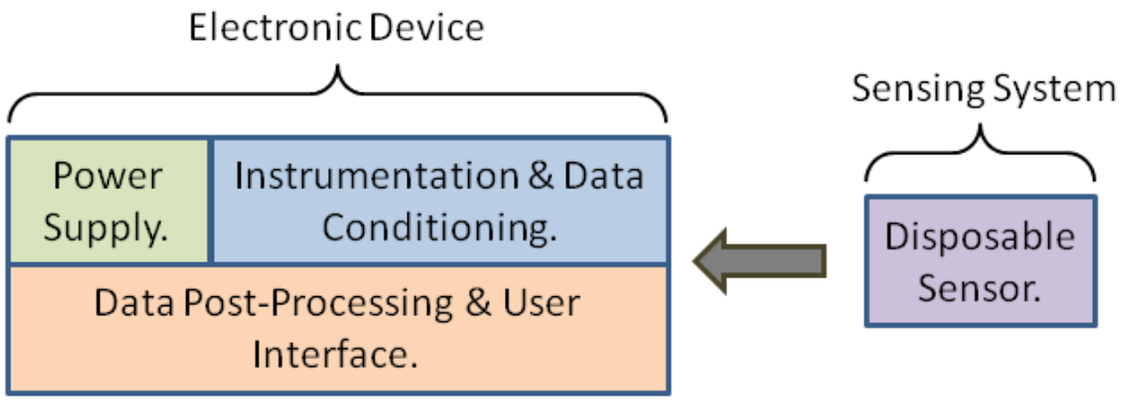

Figure 2. PoC device schematic development view.

2. Point-of-care device electronics design

2.1. Front-end electronics depending on the sensing topology

As it has been stated before, there are different electrodes topologies for the sensing system implementation, depending on the system and applications requirements. Different configurations must be designed for the front-end electronics architecture depending on the sensing topology.

In case of a three-electrode sensing topology, the potentiostat is the key electronic component for this sensing configuration, which is the interface between the biological elements and the instrumentation electronics. The potentiostat can be implemented in different ways, especially in terms of electrodes current, which can be designed as an instrumentation amplifier current readout stage or a transimpedance amplifier readout stage [16].

In figure 3A, a simple potentiostat with an instrumentation amplifier readout stage has been shown. It consists of an operational amplifier (OA), which tracks the input signal (V_{IN}) on to electrodes, and an instrumentation amplifier (IA) that senses the current through the electrodes.

http://dx.doi.org/10.5772/60843

$$I_{CELL} = \frac{V_{IN}}{Z_{CELL}}$$

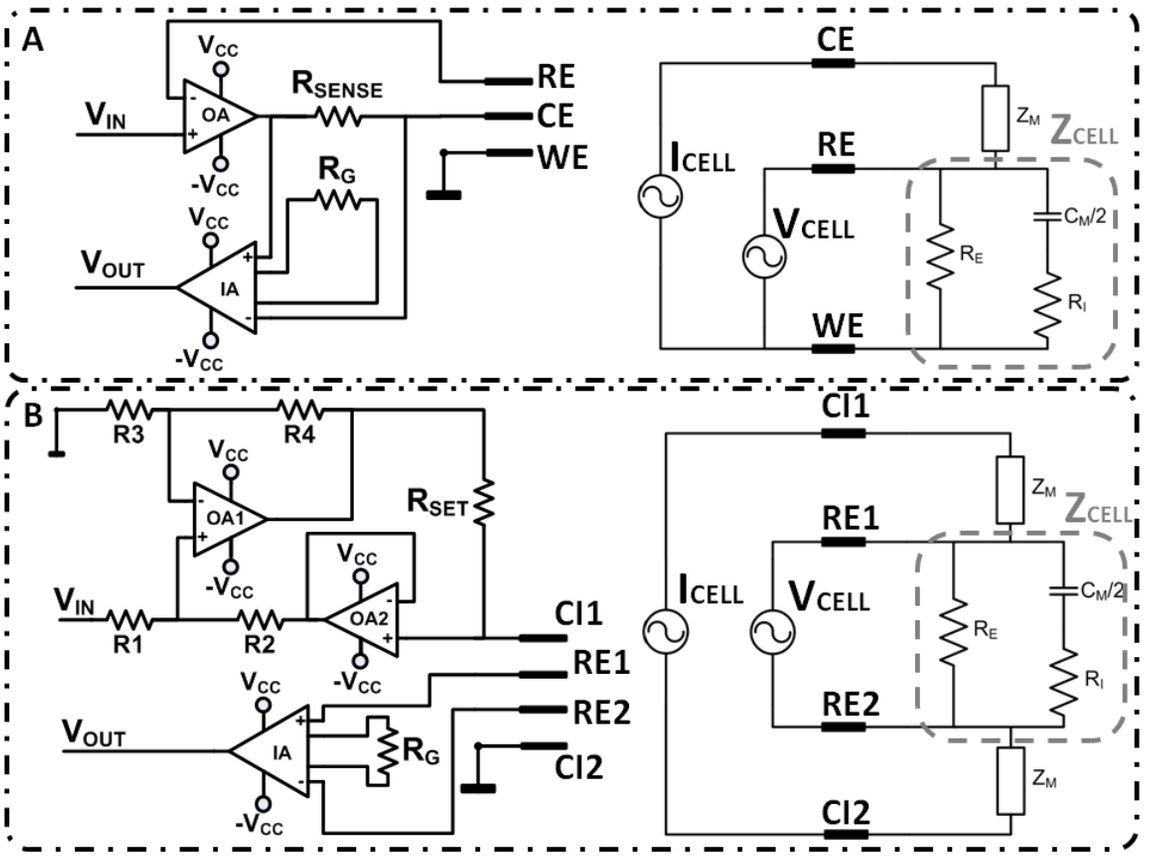

Figure 3. Cellular model, sensing system, and front-end electronics. A: 3-electrode cofiguration. B: 4-electrode configuration.

The current readout electronics consists of the direct conversion of the current through the biological species (I_{CELL}) into a voltage signal by means of a resistor (R_{SENSE}), where an instrumentation amplifier measures the voltage difference. The current through resistor (R_{SENSE}) is equal to the current through the biological species (I_{CELL}), and the voltage between RE and WE is steady due to the direct connection of WE to ground reference. Instrumentation amplifier's gain has been set to 1 to optimize the amplifier's total harmonic distortion.

$$Z_{CELL} = R_{SENSE}\left(\frac{V_{IN}}{V_{OUT}}\right)$$

In case of a four-electrode configuration, a voltage-to-current converter is implemented. In Figure 3B, the voltage-to-current converter is a modified Howland cell based on operational amplifiers (OA1 and OA2), which must guarantee a wide bandwidth and a high slew-rate

while maintaining a low spectral noise and a low offset performance. The Howland cell uses R_{SET} and the input signal (V_{IN}) amplitude to define a stable current signal (I_{OUT}) at the output of the circuit regardless of the connected load related to the biological species.

$$I_{CELL} = \left(\frac{1}{R_{SET}} \right) V_{IN}$$

The differential voltage between ER1 and ER2 electrodes is acquired by means of the instrumentation amplifier (IA). The measured voltage (signal V_{IS}) is related to the differential voltage between the reading electrodes (ER1 and ER2), G being the instrumentation amplifier gain.

$$V_{OUT} = G\left(V_{ER1} - V_{ER2}\right) = G.\left(Z_{CELL}.I_{CELL}\right)$$
$$Z_{CELL} = R_{SET}\left(\frac{V_{OUT}}{G.V_{IN}}\right)$$

2.2. Back-end electronics for data post-processing and user interface

The sensing topology and front-end electronics chosen for the implementation of the PoC device outputs a voltage signal related to the biological impedance, which is of complex magnitude. The purpose of the back-end electronics, independent of the front-end electronics and sensing system, is to supply the proper voltage signal to bias the instrumentation electronics, depending on the biological sample, sensor, and experimental setup; process the output data; and present a proper user interface.

Taking into account these considerations, the first approach based on impedance spectroscopy (IS) is a versatile solution in different topics and environments. Two different approaches can be considered for the IS method; the Fast Fourier Transform (FFT) [17] method and the Frequency Response Analyzer (FRA) [18]. In the FFT method, a pulse is applied, ideally a Dirac delta function, to the sample and considering that it contains a wide frequency content, the response provides a full spectrum data of the analyzed sample impedance. The front-end electronics response is analyzed with an FFT algorithm in order to extract the frequency components of the impedance spectra [17]. This method is a simple and fast solution for the IS, but there are several drawbacks in the implementation. It is very difficult to generate a fast step function and a very fast electronic instrumentation capable of driving this step on the electrodes and extracting the resulting signal, producing a distortion in the measurement. Moreover, the important impedance information is contained in a short period of time after the step is applied; so, in addition to a very fast electronic instrumentation, a very fast analog-to-digital converter (ADC) with a high-precision bit resolution is also required, resulting in a high-speed hardware and heavy algorithm implementation device. Considering the PoC characteristics of the device, the FRA approach is a simpler and more efficient solution based on a lock-in amplifier (LIA). This method is much slower, as every frequency component is analyzed separately, to obtain the Bode plot of the measured impedance. The FRA solution is

http://dx.doi.org/10.5772/60843

a good solution in terms of the trade-off between speed and complexity, particularly if not too low frequencies need to be measured, as it actually happens on biological cellular samples [3, 5, 19, 20]. Moreover, the implementation of a LIA is useful to reject undesirable harmonics and noise interferences [21-23], which are predominant on biological environments, such as bacteria culture, saline solution buffers, blood plasma, etc.

Complete back-end electronics have been designed to perform the FRA solution based on a real-time mathematical processing digital lock-in amplifier (DLIA) embedded on a real-time platform sbRIO 9632 (National Instruments, Austin, TX, USA), which has been used for fast software prototype development and versatility. To perform the FRA analysis based on a DLIA, the biasing signal of the front-end electronics (V_{IN}) is adopted as a reference signal to analyze the response of the sensing system (V_{OUT}). The sine and cosine signals are derived from V_{IN}, and by means of two multipliers and a filter stage, the real and imaginary components of V_{OUT} are obtained [16] (Figure 4). This measurement must be done for each frequency and front-end electronics output signal to obtain the Bode plot which consists of its magnitude $|V_{OUT}|$ and phase φ_{OUT}, where V_{REAL} and V_{IM} are the real part and imaginary part of the output signal, respectively.

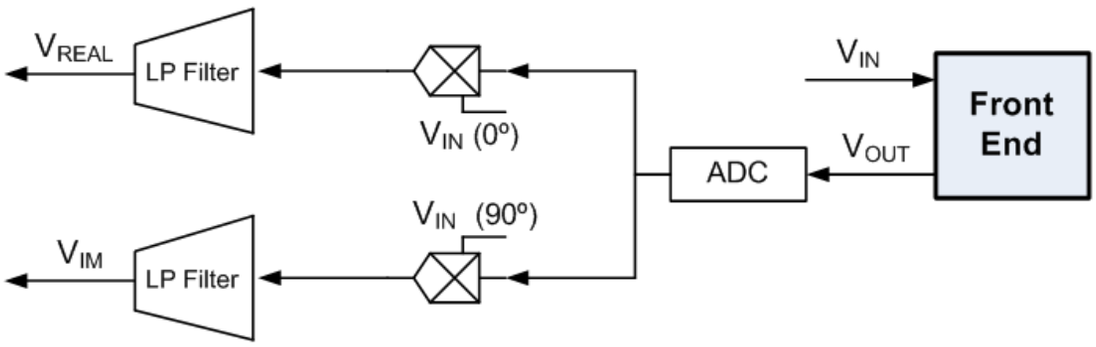

Figure 4. Lock-in software diagram. V_{OUT} is the input signal coming from the front-end electronics, V_{IN} is the reference signal and V_{REAL}, V_{IM}, respectively, are the real and the imaginary parts of the sensing system response.

$$V_{OUT} = \frac{4\sqrt{\left(V_{REAL}^2 + V_{IM}^2\right)}}{V_{IN}}$$

$$\varphi_{OUT} = \arctan\left(\frac{V_{IM}}{V_{REAL}}\right)$$

$$V_{REAL} = \frac{1}{2} V_{OUT}.V_{IN}.\cos\left(\varphi_{OUT}\right)$$

$$V_{IM} = \frac{1}{2} V_{OUT}.V_{IN}.\sin\left(\varphi_{OUT}\right)$$

Figure 5 depicts the back-end electronics architecture for the IA device. It is composed by the sbRIO 9632 real-time platform that allows us to develop different back-end functionalities,

such as an oscillator (OSC) (Figure 5) that provides the desired biasing signal (V_{IN}) for the front-end electronics, and the signal conditioning for dual analog-to-digital conversion of both V_{IN} and V_{OUT} signals needed for the FRA approach. The oscillator is based on a signal generator AD9833 (Analog Devices, Norwood, MA, USA) that provides a stable voltage signal with a wide variable frequency range, 0 MHz to 12.5 MHz, which is controlled by a serial peripheral interface (SPI) communication protocol. The signal conditioning consists of a 12-bit dual, low power consuming ADC (Figure 5) known as ADC12D040 (Texas Instruments, Dallas, TX, USA), capable of converting both analog input signals at 40 MSPS simultaneously. The analog inputs are converted from single-ended input to differential output with a differential amplifier (Figure 5) AD8138 (Analog Devices, Norwood, MA, USA).

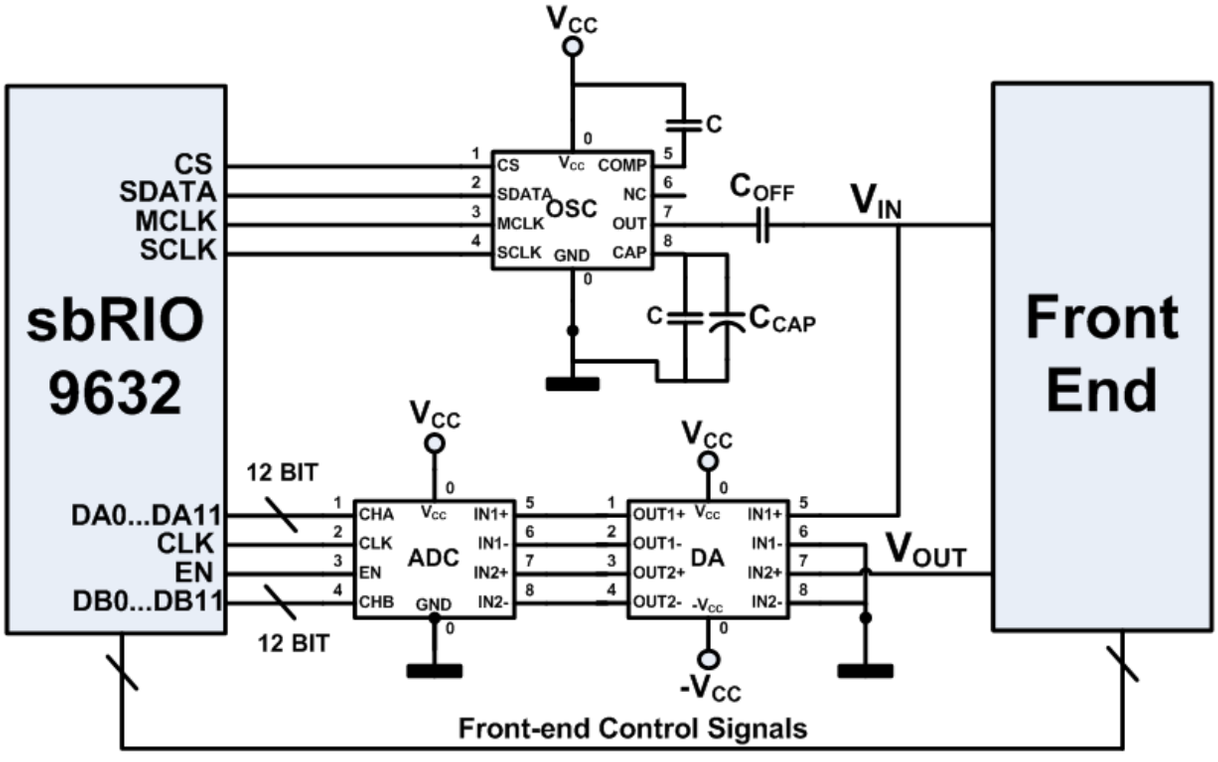

Figure 5. Back-end electronics based on a real-time platform sbRIO 9632.

Finally, a software for system control, data processing, and user interface is embedded on the real-time platform, which offers several functionalities.

First of all, it provides steady clock signals as needed that can be automatically real-time adjusted, allowing complete parallel signal acquisition for all the frequency ranges and more precise control of the oscillator, enabling the development of a signal generator automatic frequency sweep for an automated and complete FRA.

Furthermore, some functionalities on the front-end electronics, like R_{SENSE} or R_{SET} multiplexed auto-scale, are basic features for a precise FRA method and can be implemented by means of additional digital control as it is depicted in Figure 5 (front-end control signals). The real-time

http://dx.doi.org/10.5772/60843

platform allows the system configuration and data display, with a user-friendly front-end user panel using Labview (National Instruments, Austin, TX, USA), by means of an external computer connected to the platform with a standard Ethernet connection.

2.3. Back-end electronics test

DLIA is the key component of the whole back-end electronics system, and must be capable to extract information from highly contaminated signals provided by the sensing system, usually electrical signals buried in noise. To estimate the signal-to-noise ratio (SNR) of the DLIA; the parameter that quantifies the ability of the DLIA to extract information of highly contaminated signals; a signal of 10 mV amplitude had been injected at the back-end electronics input V_{OUT}, as the information signal to be processed, for different frequencies ranging from 10 Hz to 100 kHz. Different noise signals representing different noise amplitude values had been added to the information signal for two different frequencies, 50 Hz and 200 kHz.

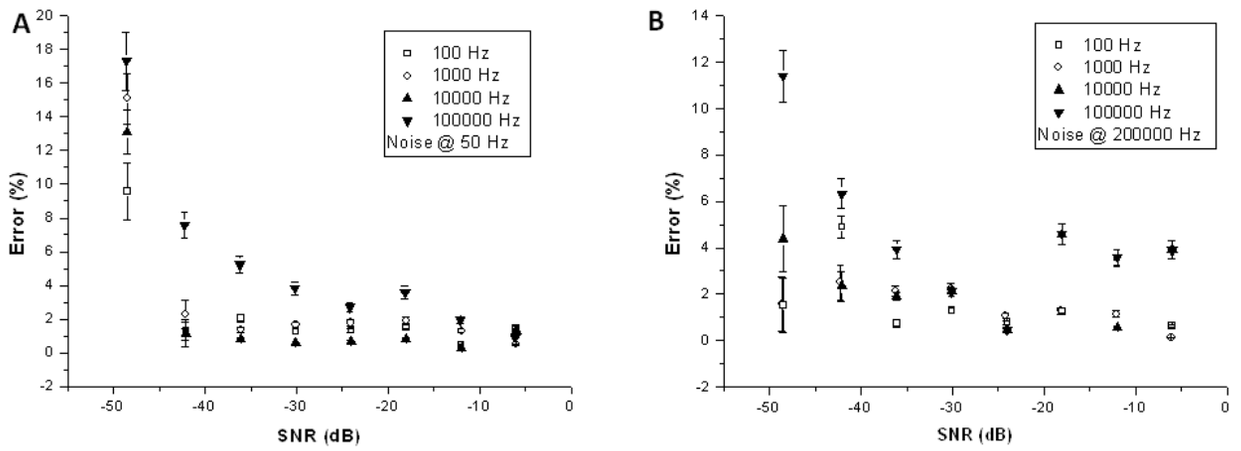

Figure 6. System response to a resistor impedance measurement. A: 50 Hz, low-frequency noise signal. B: 200 kHz, high-frequency noise signal.

Figure 6 shows the error and standard deviation when recovering the information from the different noise-contaminated 10 mV electrical signal. Measurement errors are below 10% for signal-to-noise ratio up to -45 dB, noise levels 200 times higher than the signal amplitude, which means a great environmental noise rejection for both lower (50 Hz) and higher frequencies (200 kHz).

2.4. Combined front-end and back-end electronics test using passive components

The complete PoC device combining both front-end instrumentation for sensing system driving and back-end electronics for data processing and device control, have been tested using passive components (Figure 7). The three-electrode front-end architecture, based on a potentiostat, has been selected for these studies, as three-electrode commercial sensors will be used later. Moreover, the passive components used in the study are in the ranges of typical blood

impedance values [4, 5, 8, 12, 24], as the PoC device will be later applied to particular blood analysis. The operational amplifier to bias the sensor is the AD825 (Analog Devices, Norwood, MA, USA), a dual-supply high-speed Junction Gate Field Effect Transistor (JFET) amplifier with low leakage current and low distortion capable of high output driving. The instrumentation amplifier, AD8421 (Analog Devices, Norwood, MA, USA), is a dual-supply high-speed instrumentation amplifier with low noise and ultralow bias current. The amplifier's gain has been set to 1 in order to optimize the amplifier's total harmonic distortion. This stage has been designed with four different multiplexed sensing resistors (R_{SENSE}) taking into account the expected impedance values shown in the literature between 100 Ω and 100 kΩ [4, 5, 8, 12, 24], as was subsequently confirmed in the system validation experiments. These resistors are automatically multiplexed with an auto-scale function controlled by the embedded software.

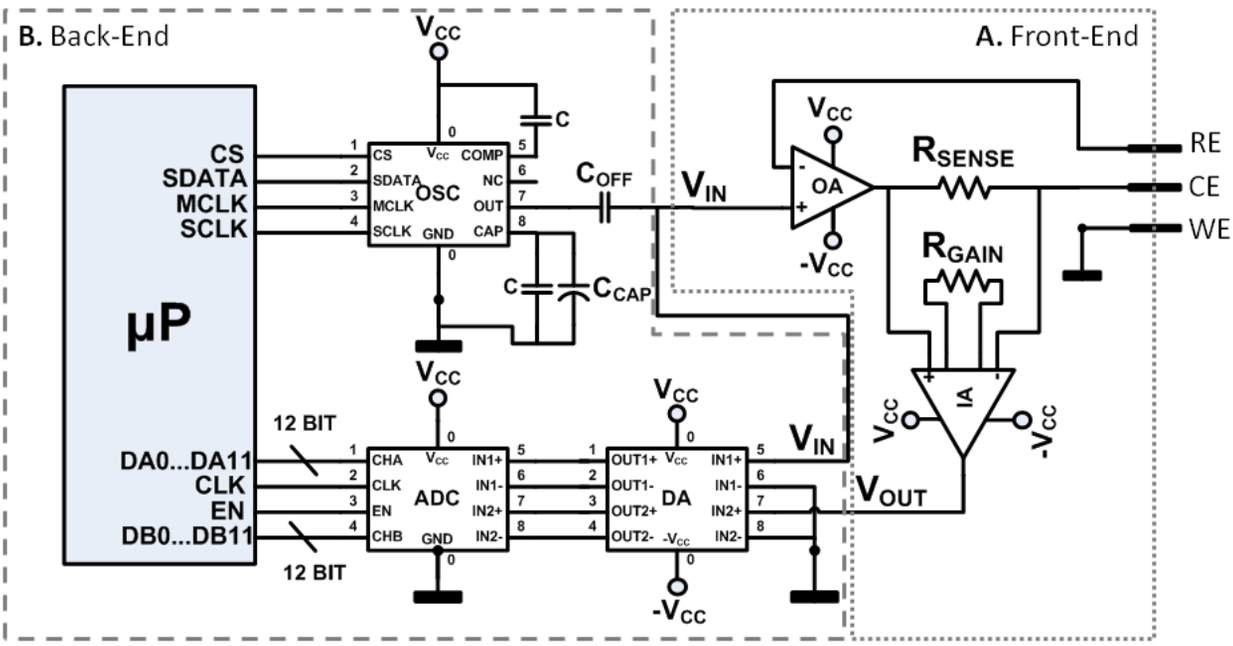

Figure 7. PoC impedance analysis device schematic diagram. A: Front-end electronics. B: Back-end electronics

First of all, we analyze a single resistor of different values as an electrode load in both impedance magnitude (Figure 8A) and phase (Figure 8B). Results demonstrate a great performance and reliability with an impedance magnitude standard deviation of 1%, maximum error of 12.3% in a 100 kHz bandwidth for loads less than 10 kΩ. For loads greater than 10 kΩ, the system performance declines with an impedance magnitude standard deviation of 3% and maximum error of 14% and bandwidth less than 10 kHz. In terms of impedance phase, Figure 8B, the system performance shows a standard deviation of 3.7 degrees in a 10 kHz bandwidth except for higher load values. The potentiostat topology causes a bandwidth limitation, as the instrumentation amplifier current readout system introduces an extra load (R_{SENSE}) on the main amplifier feedback loop, especially when the load increases.

http://dx.doi.org/10.5772/60843

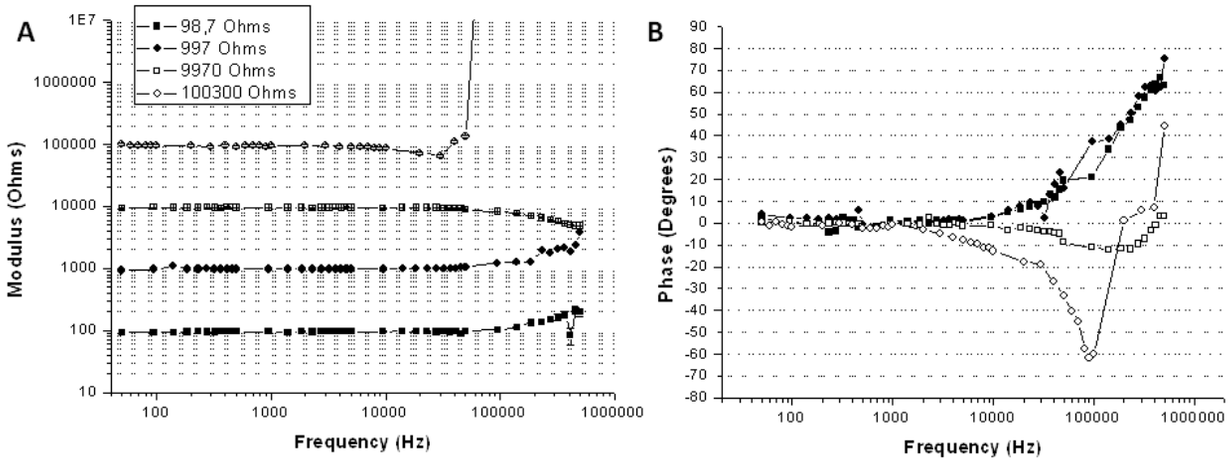

Figure 8. System response for a different resistor values. A: Impedance magnitude. B: Impedance phase.

A transimpedance amplifier topology [16] may solve this problem, as the current readout system and the sensing resistor (R_{SENSE}) are placed outside the feedback loop of the main amplifier. However, the generation of a voltage reference on the electrodes is based on a virtual ground provided by the transimpedance amplifier (Figure 9B), leading to possible errors on electrodes biasing [16].

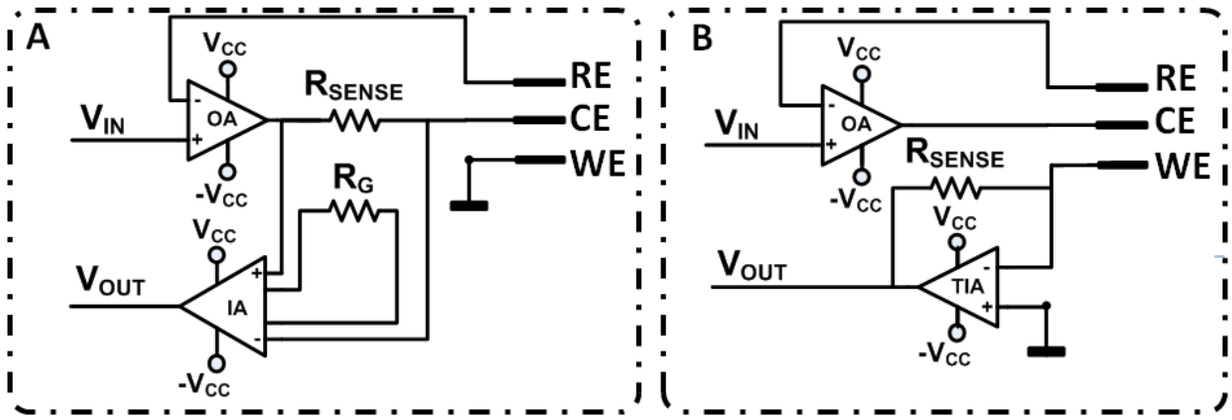

Figure 9. Potentiostat topologies. A: Instrumentation amplifier current readout topology. B: Transimpedance amplifier current readout topology.

Moreover, presence of stray capacitances creates a high-frequency measurement deviation called "Hook Effect." It is caused by leaking currents on the instrumentation [25], producing an impedance measurement error that can be observed above the 100 kHz. This error is frequency and load dependant, as leaking current paths through parasitic capacitances is more conductive at high frequencies and loads. In spite of these limitations, it is not a major drawback to the PoC device application, because the typical impedance and working frequency values for HCT analysis found in literature are below the described limitations [4, 5, 8, 12, 24].

Finally, the whole PoC device has been tested adopting a parallel resistor and capacitor as a load configuration (Table 1). Figure 10 shows the impedance magnitude and phase, in comparison with the theoretical load behavior. Three different resistor and capacitor values have been tested:

	Resistor Value.	Capacitor Value.
Test 1	597Ω	9.98nF
Test 2	994Ω	3.86nF
Test 3	9940Ω	9.98nF

Table 1. Load values.

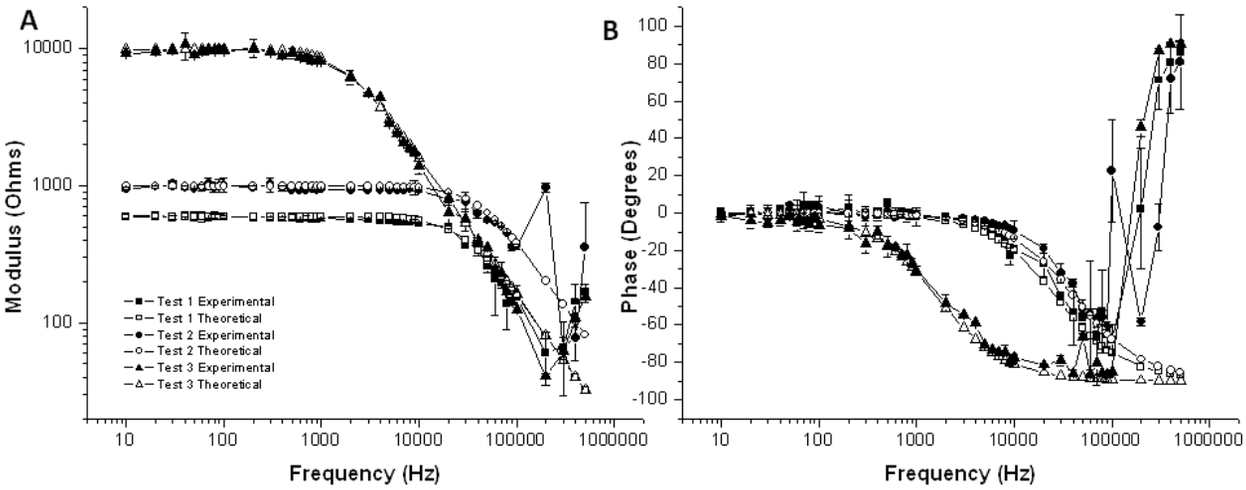

Figure 10. System response for a different parallel resistor and capacitor values. A: Impedance magnitude. B: Impedance phase.

Results in Figure 10 show a great performance with an impedance magnitude standard deviation of 1.5%, a mean error of 3.5% with a defined 100 kHz bandwidth.

2.5. Combined front-end and back-end electronics test using a ferrocyanide/ferricyanide solution

Finally, the whole PoC device has been validated for different sensors topology and compared the device measurements with a commercial equipment SP-150 (BioLogic Science Instruments, Grenoble, France) using a ferrocyanide/ferricyanide solution, a commonly used substance on sensor and equipment characterization [26-28].

Two different sensors have been used: a disposable commercial three screen-printed electrode C223AT (DropSens, Llaneras, Spain); and a standard three-electrode laboratory sensor

http://dx.doi.org/10.5772/60843

composed by three different probes. Figures 11A and 11B show the impedance magnitude and phase comparison between the developed device and the commercial equipment SP-150, using the same disposable three screen-printed electrode (C223AT).

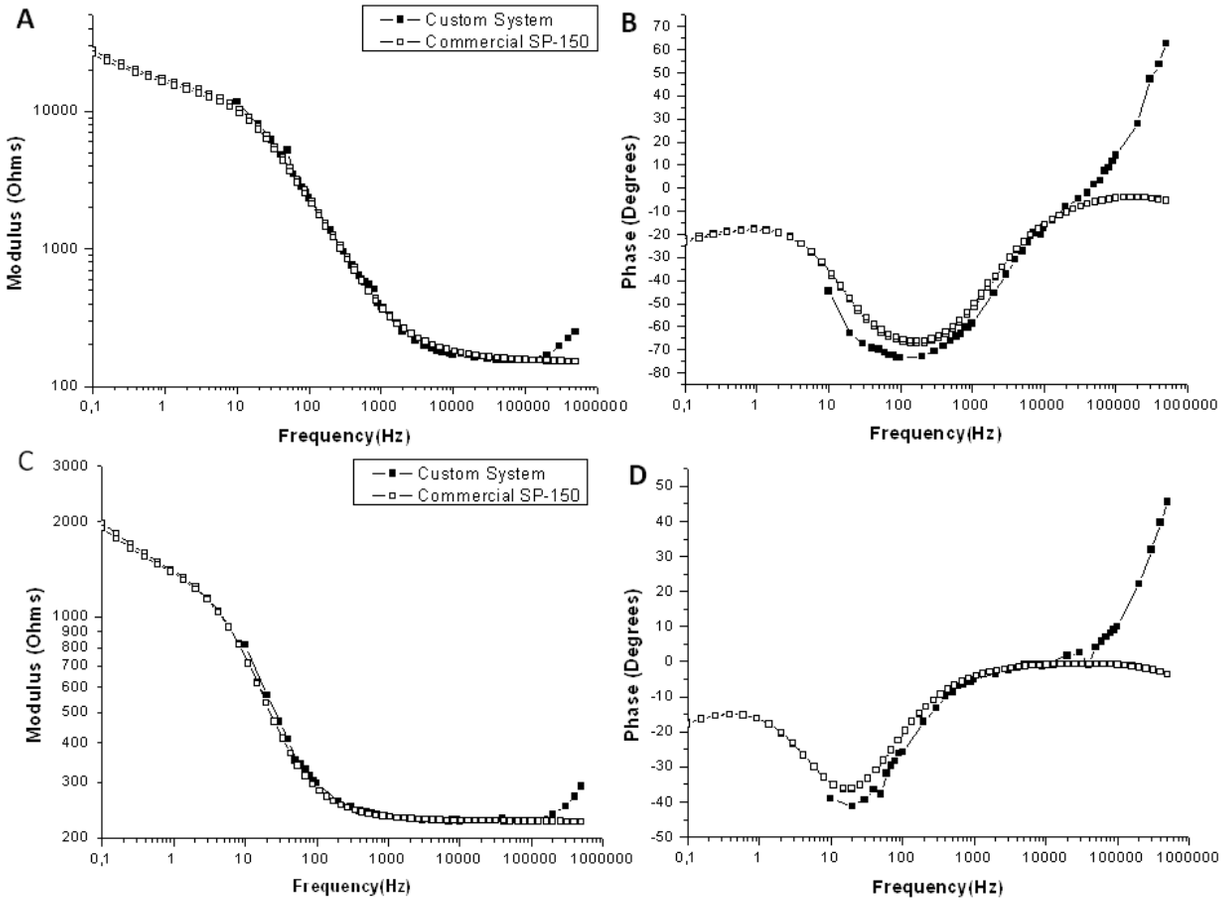

Figure 11. Comparative results with commercial equipment SP-150. A: Commercial sensor C223AT impedance magnitude. B: Commercial sensor C223AT impedance phase. C: Standard laboratory probe impedance magnitude. D: Standard laboratory probe impedance phase.

Figures 11C and 11D show the impedance magnitude and phase comparison between the developed device and the commercial equipment SP-150 using the same standard laboratory three probe electrodes sensor for all the experiments. The system has a proper impedance measurement response in the frequency operating range from 10 to 100 kHz, working within the ranges described earlier, with an impedance magnitude standard deviation of 1% and a maximum error of 1.5%. In terms of phase, maximum error is less than 12.1 degrees and the electrodes electrical pole positions represented are at accurate position. A final system characteristics summary is reported in Table 2:

	Conditions (T = 25ºC)	Value
Power Consumption		24 VDC 0.35 A
Applied Voltage Signal Amplitude		10 Vrms
Frequency Working Range	Load < 10 kΩ	< 100 kHz
Frequency Working Range	Load > 10 kΩ	< 10 kHz
Magnitude Maximum Error	In Frequency Working Range	< 12.3%
Phase Maximum Error	In Frequency Working Range	< 12.1º
Lock-In Average SNR Rejected		-43 dB

Table 2. System characteristics summary.

3. Point-of-care device for anemia detection using commercial disposable sensors

3.1. Introduction to anemia

In this section, the previously reported PoC solution is studied for the detection of anemia through whole blood HCT monitoring, using a plug-and-play low-cost disposable commercial sensor.

Anemia is defined by the World Health Organization (WHO) as the stage at which the amount of hemoglobin in blood is below a certain threshold, being considered a world-wide problem [29]. HCT is the proportion of blood volume occupied by red blood cells (RBCs) and is determined by cell number and size, so HCT values below a certain reference range may also indicate anemia or abnormal cell development. 1.62 billion people (24.8% of the global population) are affected by anemia. The highest prevalence of anemia is in less developed countries, such as Africa and south-east Asia (~65%), and around 20% in developed countries, such as the Americas, Europe, and Western Pacific [30]. Severe anemia can lead to major health consequences such as pregnancy disorders, poor physical and cognitive development, and increased risk of morbidity, while less severe cases provoke weakness, fatigue, and dizziness [30, 31]. Nutritional deficiencies, such as severe malnutrition [32], colon cancer [33], or gastrointestinal lesions [34], are the most common cause of anemia, while other anemia originators are hematologic diseases such as sickle cell anemia [35] or thalassemia [36], cancer treatments (chemotherapy and radiation) [37], and indirect causes, such as lower erythropoietin production [38]. Also, frequent blood donations and huge blood draws from hospitalized patients may induce anemia [39]. Non-invasive methods are being studied and developed for anemia screening but have been demonstrated to have lower precision and sensitivity level [40, 41].

These different factors push toward the development of PoC anemia equipment providing an easy-to-use, reliable, and sensitive test with a short response time relying on 50 μL blood

sample, which can be collected from capillary by standard medical procedures [42], providing reduced disposition decision time [43] and replacing current venipuncture-based laboratory test and improving patient satisfaction [44]. Moreover, low-volume blood samples avoid inducing anemia or making it worse, as phlebotomy is reported to induce anemia in hospitalized patients [45].

Currently, non-specific huge laboratory devices utilize IS-based applications, involving complex experimental setups and significant expenditure of time. Furthermore, whole blood PoC specific sensing systems also rely on complex microfluidic devices [46] entailing a low environmental integration level to develop autonomous PoC applications [47]. Moreover, IA measurements were performed at 10 mV_{RMS}, to prevent undesired effects like electroporation or irreversible electrical breakdown, which will damage RBCs membranes [48].

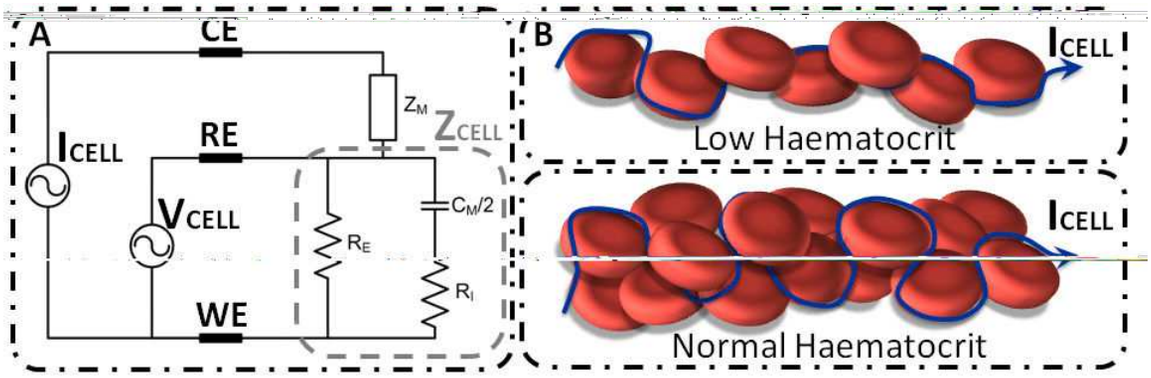

Figure 12. Red Blood Cell (RBC) electrical model. A: Three-electrode model for RBC sample. B: Current flow path through different blood samples with different hematocrit.

The electrical model for dilute cell suspensions in a three-electrode sensor (Figure 12) can be described as an electrical components network, where the close relation between HCT and impedance at low frequencies (up to 100 kHz) has been confirmed [49]. At this frequency range, the current I_{CELL} flows outside the RBCs, across RE impedance. HCT increment on the sample makes the current flow path larger between RE and WE electrodes, becoming an increment on Z_{CELL} impedance. According to literature, this phenomenon occurs at the 10 Hz to 100 kHz frequency range [2, 49].

3.2. Sensor

The sensing system is a low-cost disposable commercial sensor, easy to manipulate by clinical laboratory technicians using standard clinical laboratory tools. It works with 50 μL blood samples, the standard volume for a whole blood drop, easily collected from capillaries [42], and it is made of gold, an acknowledged bio-compatible material. Different commercial sensors have been evaluated, such as AC1 sensor from BVT Technologies (Brno, Czech Republic) or the G-AUG sensor series from Bio-Logic SAS (Claix, France), and the commercial sensor that best meets the defined specifications is the C223AT from Dropsens (Llaneras, Spain).

The device has a plug-and-play sensor system inside a Faraday cage and it is connected to the electronics with a custom-made three-wire coaxial insulated cable in order to provide an easy-to-use setup and reliable performance. Blood samples were put on top of the sensor with an automatic pipette (Labopette Manual 10–100 μL; Hirschmann Laborgeräte, Eberstadt, Germany).

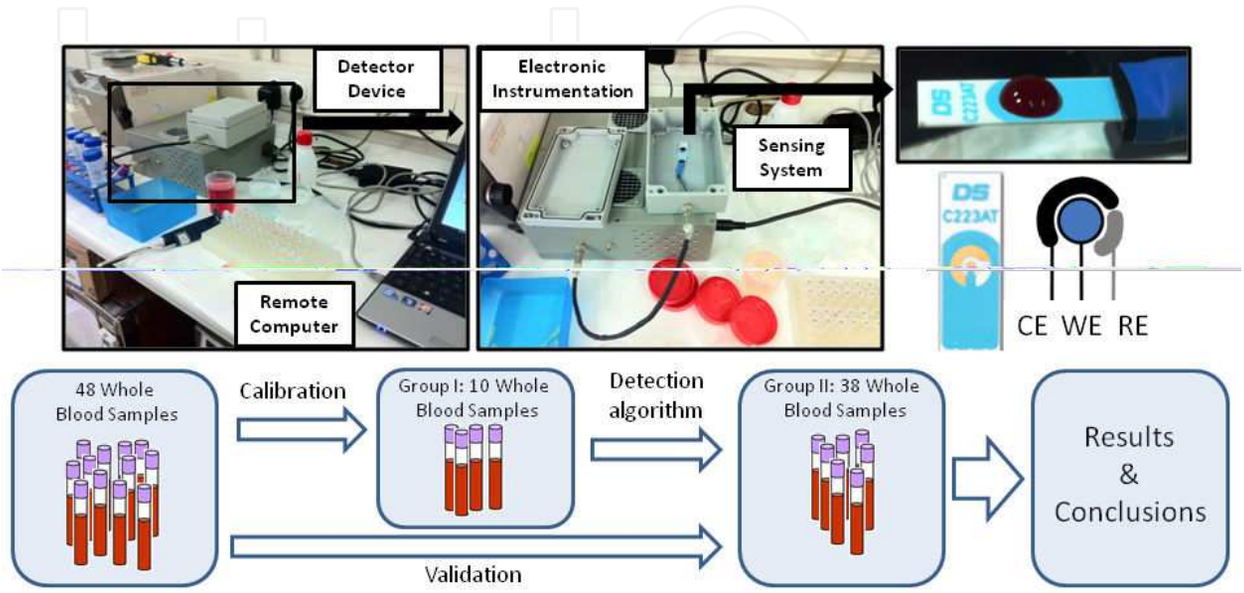

Figure 13. Device prototype electronics: Two custom printed circuit board and a sbRIO 9632 board (National Instruments, Austin, TX, USA) inside a faraday cage. Experimental setup: disposable sensor; electronic instrumentation; external computer with control and data displaying software. Whole blood samples groups and experimental procedure.

3.3. Blood samples

We used 48 whole blood samples obtained from hospitalized patients in Hospital Clínic. However, personal data of the patients was not available to the investigators and samples were randomly selected. Whole blood samples were obtained in 4 mL tubes containing ethylenediaminetetraacetic acid (EDTA 7.2 mg; BD Vacutainer®, Madrid, Spain).

We performed a complete blood count (CBC) of the blood samples with a hematology analyzer (Advia 2120, Siemens AG, Madrid, Spain), which reported the hemoglobin and HCT results as g/dL and percentage (%), respectively. With this methodology, the blood sample stream is divided into two parts, one portion is used for RBC counting and size and other portion is used for hemoglobinometry. RBC counting and size analysis is performed by singly passing the RBCs through a small direct current, where the temporary increase in impedance provides the information about number and volume. HCT is calculated from the measured RBC number and volume [50].

These 48 whole blood samples were distributed in two different groups (Figure 13). The first one (group I), consisted of 10 samples, was used to calibrate the system, whereas the second one (group II), composed by the other randomly collected 38 whole blood samples, was used

http://dx.doi.org/10.5772/60843

to validate the whole system performance. The samples in group I have been selected to cover the entire possible HCT range present in human blood.

3.4. Software description

A user-friendly front-end panel on a remote computer has been designed for system configuration and data display. The real-time platform allows us to connect our device to a remote computer by means of a standard Ethernet connection. The user panel, depicted in Figure 14, has two different configurations that can be selected from a menu (A label). Each option allows the system to perform different experiments when the start button (D label) key is pressed. The first one is a complete impedance spectroscopy that provides the Bode diagrams for both impedance magnitude (F label) and phase (G label), where the user could choose the number of points per decade (C label). IA frequency ranges are fixed to the defined bandwidth on section 3.2 and R_{SENSE} values are auto-scaled. The second is an automatic HCT analyzer, where the blood sample HCT is displayed with four significant numbers (B label).

Figure 14. Software front panel for system control and data displaying.

Moreover, the front panel has several displays for user control and error monitoring. The two signals needed for the FRA analysis, reference signal (V_{IN} in Figure 5), and measurement signal (V_{OUT} in Figure 5), are real-time monitored and shown on a graph (E label). Errors in electronics

connection with the remote computer are displayed (H label) and generic Labview errors are explained (J label).

3.5. Anemia detection device validation

3.5.1. System calibration: IA spectra analysis

The designed device was validated through IS experiences with the specified sensor described, for each whole blood sample collected, with all the measurements performed at clinical laboratory room temperature. First of all, we measured a complete impedance spectrum for the group I whole blood samples.

The obtained impedance magnitude (Figure 15A) and phase (Figure 15B) Bode diagrams for whole blood samples demonstrate that there exists a difference between measurements for different samples in specific frequency ranges. Furthermore, these differences must be related to whole blood HCT, as the response current I_{CELL} flows outside the RBCs, as discussed in previous section. When HCT is higher, the current flow path becomes larger between the RE and WE electrodes, which represents an increment on measured Z_{CELL} impedance. Therefore, measured impedance differences must be defined as impedance increments related to HCT increments. This phenomenon is present on specific frequency ranges depending on the correlation between impedance measurement and HCT. In terms of impedance magnitude (Figure 15C), the frequency working range is from 10 kHz to 100 kHz and for impedance phase (Figure 15D), it is in the range from 1 kHz to 5 kHz.

The capacity of determining impedance magnitude and phase differences for different HCT samples on a wide frequency working range gives flexibility and data redundancy to the system device, as long as it is not single frequency response dependant, which makes simple statistical data analysis techniques, such as linear regression, feasible, strengthening the robustness and reliability of the device.

Hence, once we have assumed that measured impedance increments, on the defined frequency working range, are related to blood samples HCT increment, we must determine the system's capacity for detection, resolution, and sensitivity. A control software, embedded on the microprocessor from the real-time platform sbRIO 9632, has been created to instantly measure impedance on the previously defined frequency working range, and we have studied the sensitivity, accuracy, and coefficient of variation of the device.

3.5.2. System calibration: Automatic hematocrit detection

To determine the system accuracy, sensitivity, and coefficient of variation, the first approach to the detection system evaluates only the impedance magnitude measurements. Although impedance phase measurements may be related to HCT, as it is shown in Figure 15D, these values, unlike the impedance magnitude, are strongly frequency dependant, so more complex data analysis is needed, resulting in a more complex and slower system. To calibrate the system, the impedance magnitude measurements of the whole blood samples from group I will be compared with the HCT values (%) (Figure 16.). The relation of impedance magnitude

http://dx.doi.org/10.5772/60843

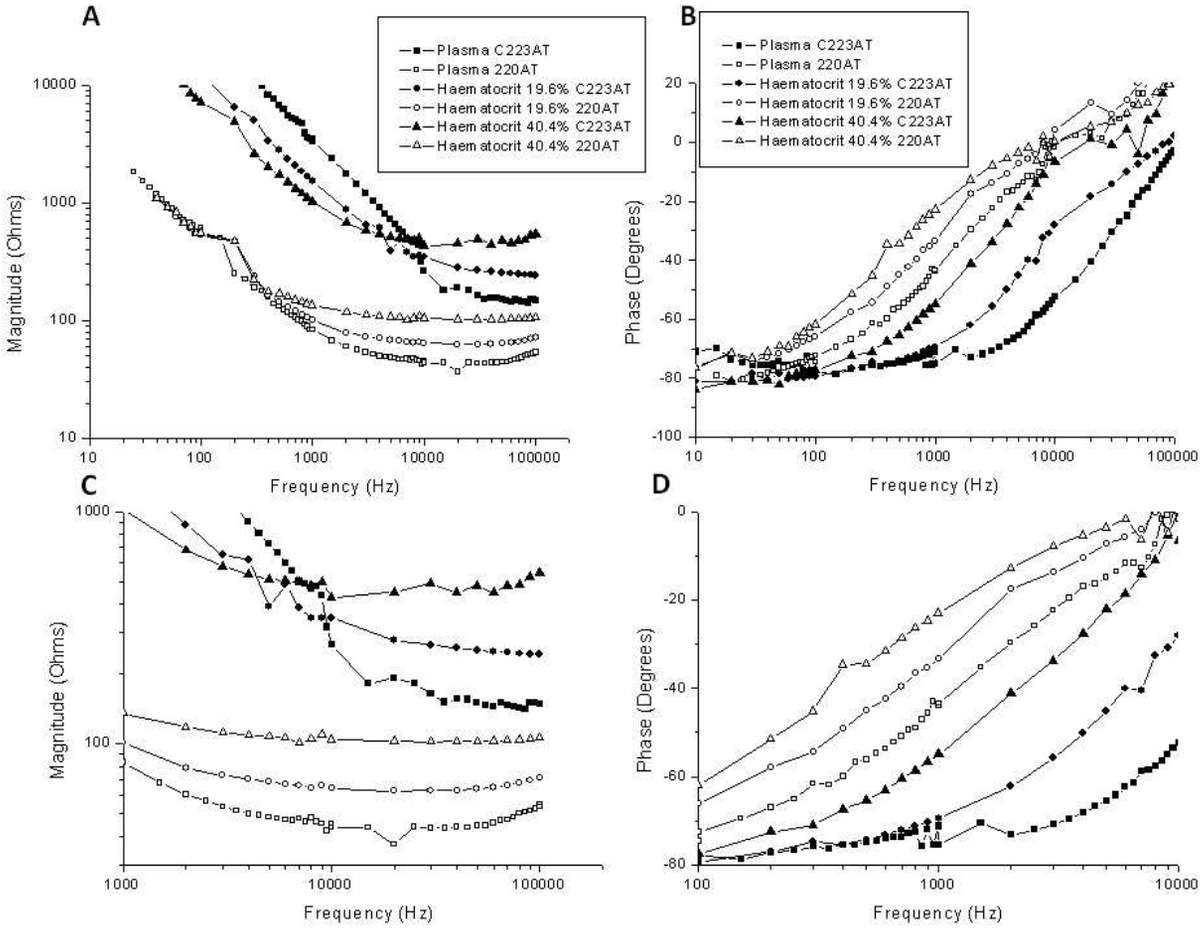

Figure 15. Whole blood impedance magnitude and phase measurement for group I whole blood samples. A: Impedance magnitude over full frequency spectra. B: Impedance phase over full frequency spectra. C: Impedance magnitude over frequency working range. D: Impedance phase over frequency working range.

($|Z|$) mean value and whole blood samples HCT had been analyzed using linear regression approach, where the slope (β_Z) defines the sensitivity, in terms of ohms per HCT percentage (Ω/%).

Meanwhile the HCT detection accuracy (%) is the relation between the linear regression standard deviation and β_Z. Precision can be evaluated with the coefficient of variation, that is, the standard deviation divided by the mean value of the five repetitions measurements. In Figure 16, the impedance magnitude for the different HCT values is depicted. The HCT detection system has 10.46 Ω/% sensitivity and a 1.13% accuracy error with a linear correlation of 0.987. The coefficient of variation of the system is acceptable as it is normally below 5%.

3.5.3. Whole blood hematocrit detection validation

Once the whole system has been calibrated, and we have confirmed the HCT relation with impedance measurement, in both magnitude and phase, with the data from these previous studies, we have implemented an automatic real-time anemia detection device that provides instantaneous HCT measurement. An HCT (%) evaluation algorithm, based on impedance

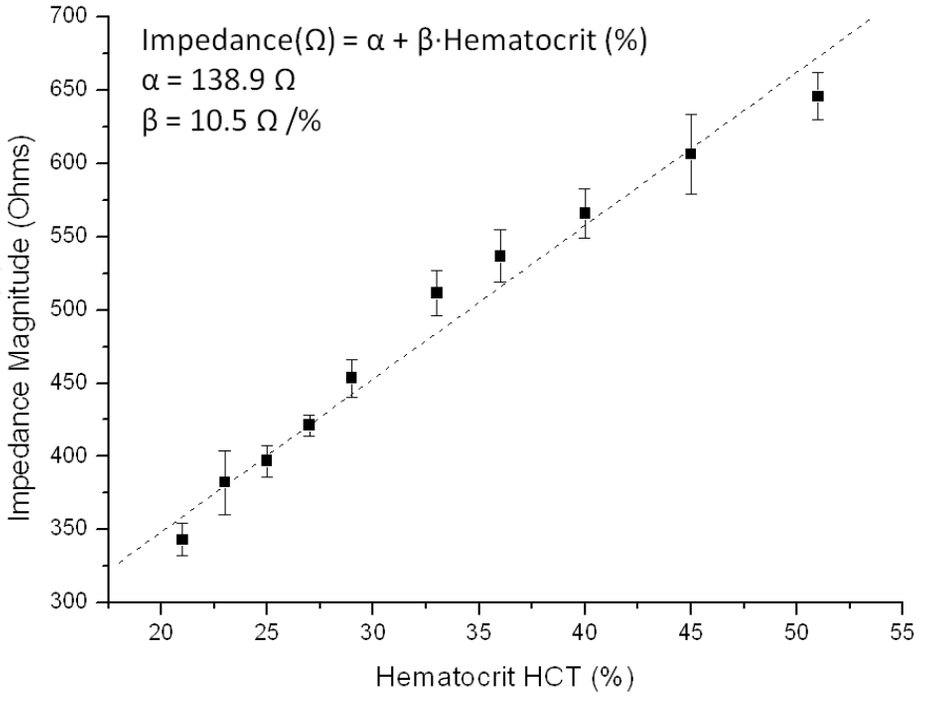

Figure 16. Measured impedance magnitude as a function of whole blood samples HCT value (%). Calibration curve.

magnitude measurement, has been embedded on the microprocessor from the real-time platform. The accuracy, precision, and repeatability of the detection device will be evaluated using 38 whole blood samples from the validation group, described in previous section (group II), which were randomly collected. Five repetitions have been done for each whole blood sample, using different sensors and sub-samples, to evaluate the precision of the device. The predicted HCT from the detection device is the mean value of the five measurements performed with each whole blood sample, and it was compared with the HCT measurement of the CBC performed with the hematology analyzer (Advia 2120, Siemens AG, Madrid, Spain).

In Figure 17, a comparison between detected HCT and HCT calculated with a clinical hematology analyzer is shown. The proposed device presented great accuracy in detecting HCT, with a linearity of 0.93 and an accuracy error of 1.75% with a correlation of 0.98. The coefficient of variation has a mean value of 3.27% for the whole samples, without any particular case with value more than 5%. In quality control procedures in clinical hematology measurements, coefficient of variation of value less than 5% for a test is considered acceptable [50]. As a first approach, which only contemplates impedance magnitude to a HCT analysis algorithm for anemia detection, as previously stated, it would be interesting to develop a more complex algorithm involving both impedance magnitude and phase on a wide frequency working range, for more precision and better performance on detection.

3.5.4. Conclusions

A first approach to a PoC device has been designed, fabricated, and tested for instantaneous anemia detection based on custom instrumentation electronics, electrical IA technique, and

http://dx.doi.org/10.5772/60843

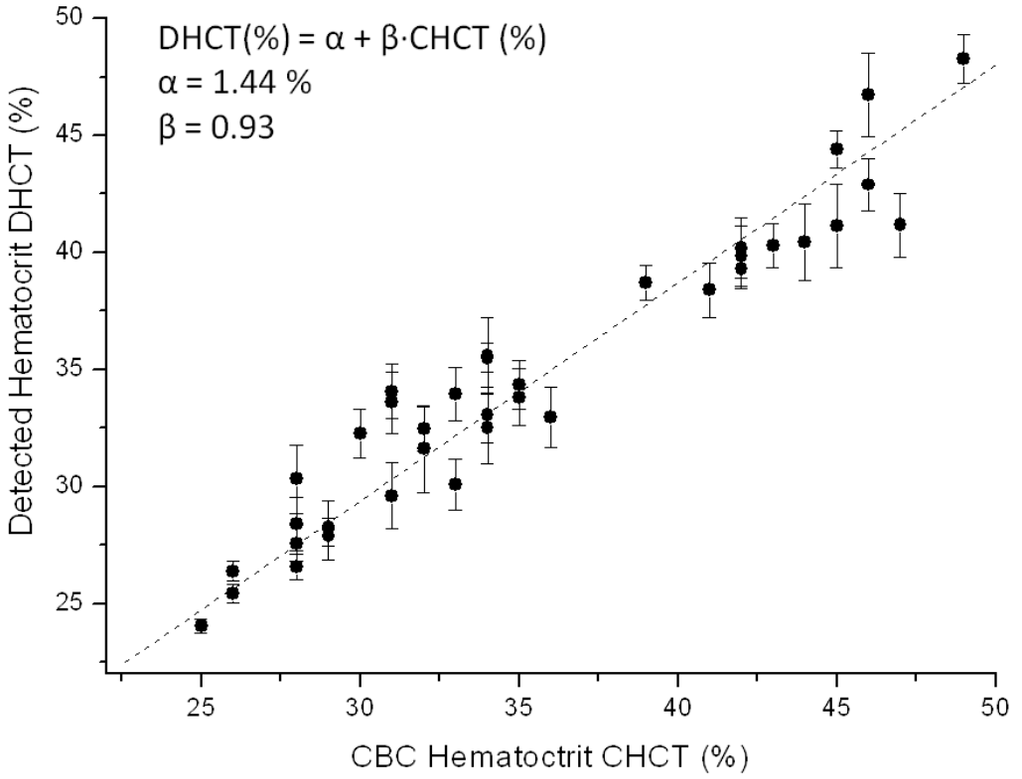

Figure 17. Whole blood HCT measurement from the detection device compared with HCT measurements obtained with a CBC performed by a hematology analyzer. Error bars represent the standard deviations across five repetitions.

disposable sensor. The system performs real-time instrumentation control, data acquisition, and results display by means of an external computer and user-friendly software. The device has been proved to exhibit reliable, robust, and effective results using label-free disposable commercial sensors using 50 μL whole blood samples. Furthermore, unlike actual clinical equipment for blood analysis, whole blood samples are not destroyed in the measurement process.

Considering this device as a first approach algorithm for anemia detection, the development of a more complex algorithm and a more accurate clinical assay with higher testing population will lead to more accurate results to assess the device performance. In addition, as the system is based on straightforward standards on instrumentation electronics and sensing, it represents an economic, portable, safe, and reliable system of anemia detection with a high degree of integration for the clinical environment.

However, further development must be considered for future stages: real-time platform sbRIO 9632 (National Instruments, Austin, TX, USA) has been used for fast prototyping purposes and versatility, but it has a major drawback in terms of power consumption, size, and price. It must be replaced by a low-cost solution for instrumentation control, data acquisition, and post-processing. The future system improvements must push toward the development of a truly autonomous, portable, and versatile device relying on the IA analysis technique.

4. Development of a truly autonomous low-cost point-of-care anemia detection device

4.1. System improvement

In this section, we will develop a truly autonomous PoC anemia detection device, based on the previous approach depicted in Section 3, as a more compact, economic, and portable PoC solution. Once the electronics and sensing system have been calibrated, the electronics involved in the data processing for a full spectrum analysis (DLIA based on FRA), such as a microprocessor, a serial peripheral interface–controlled oscillator, and a specific ADC, are no longer needed. Furthermore, a real-time platform was used which was increasing device power consumption, price and size, a major drawback when aiming for specific low-cost PoC device. The final system must be composed of an economic and reusable electronic device, with the previously reported plug-and-play disposable commercial sensor, based on three screen-printed electrodes for a 50 μL sample.

The main advantages of the proposed device are the facility of use, compactness and small size, and low-cost accessibility. These characteristics are valuable for both patients at risk of anemia and patients with chronic anemia.

Recently, other PoC anemia devices have been introduced, such as color-based diagnostic test for self-screening/self-monitoring of anemia presented by Tybursky et al. [51], which represents one of the more advanced PoC diagnostic test for self-screening/self-monitoring of anemia. This device measures hemoglobin levels, which are visually interpreted by the user using a color scale, and presents a very similar anemia detection performance compared with the device relying on IA measurements. However, there are several drawbacks to be considered; first of all, the readout stage, based on a color scale, relies on the visual interpretation of the user, which could introduce errors on the data interpretation, and reduces considerably the system resolution. Moreover, the principle of operation is based on biochemical reactions, where the blood comes into contact with a reagent solution initiating a redox reaction, which is a slow and destructive procedure.

4.2. System description

The principle of operation of the new device is the same biophysical principle of cellular IS described in Section 3. So, a full custom electronic circuit was specifically designed to carry out the impedance measurements, using a disposable three-electrode C223AT sensor (Dropsens, Llaneras, Spain), and considering the specifications of the previous study. The architecture of the device is divided in three parts: an oscillator that provides the AC voltage signal (V_{CELL}), a sensor driving instrumentation, and an RMS-to-DC converter (Figure 18).

The oscillator is based on a Wien bridge that provides a stable output amplitude signal with low distortion. The operational amplifier (OSC in Figure 18A) called AD8066 from Analog Devices (Norwood, MA, USA) is a low-cost, high-speed JFET amplifier, with low leakage current and distortion, in order to provide a stable AC voltage signal with low offset. The

http://dx.doi.org/10.5772/60843

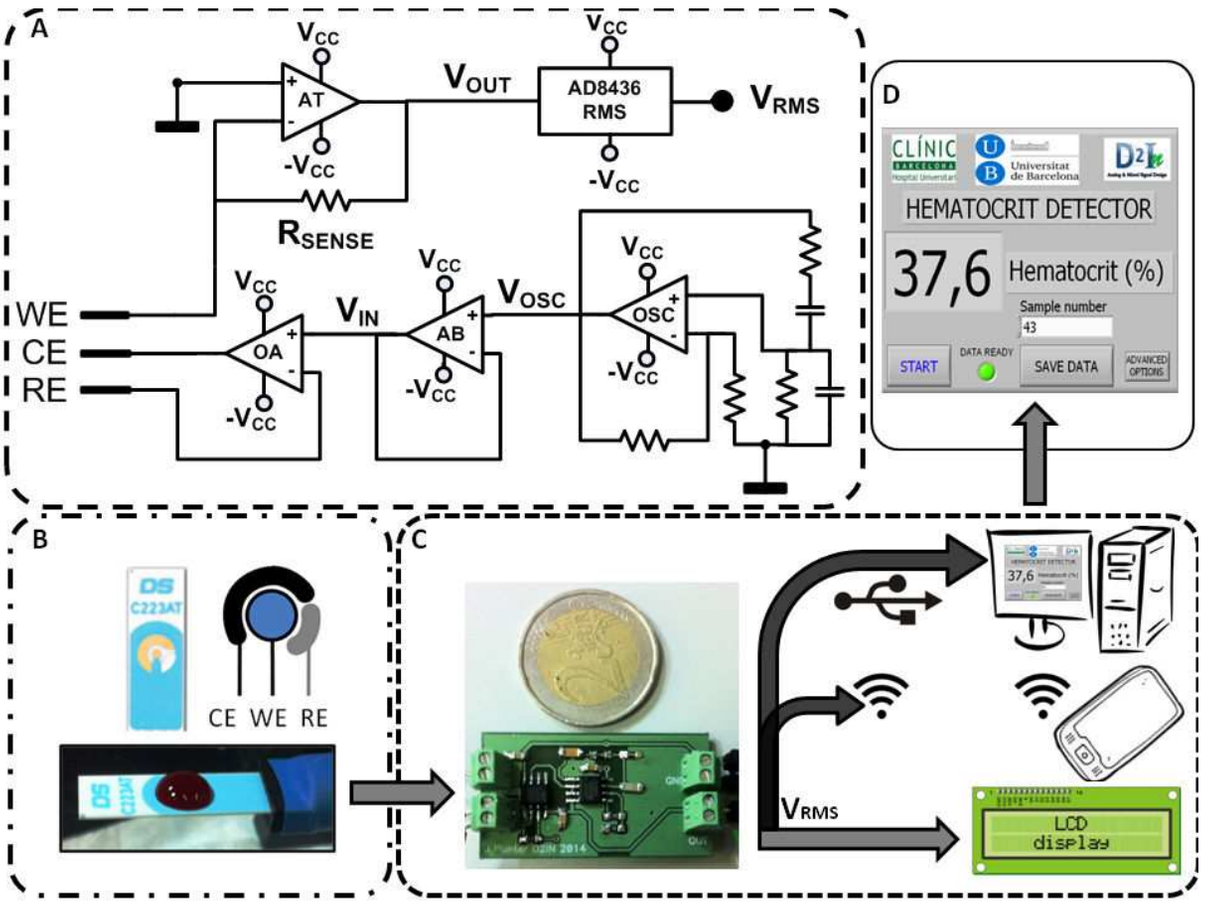

Figure 18. A: Custom electronic instrumentation. B: Commercial C223AT disposable sensor with a 50 μL whole blood drop. C: Device prototype electronics and different suitable and functional user readout interfaces. D: Actual user-friendly front-end user interface develop with Labview.

oscillator has been configured to provide a 33 kHz voltage signal, a well-suited frequency for HCT detection using the C223AT sensor. The AD8066 commercial integrated circuit provides two isolated amplifiers, so the second amplifier has been used as a follower (AB in Figure 18A) due to its high-speed and low-distortion specifications, as an isolator of the oscillator from the instrumentation.

The main electronics involved in the sensor driving is a potentiostat with a transimpedance amplifier current readout stage topology [16]. It is composed of an operational amplifier to bias the sensor and an operational amplifier in transimpedance configuration as a current readout. The operational amplifier in the potentiostat (OA, AT in Figure 18A) is the AD8066 from Analog Devices (Norwood, MA, USA), which is perfectly designed for singly driving the electrodes and track the voltage-biasing signal (V_{IN}) to the electrodes. The JFET high input impedance avoids RE electrode voltage distortion, and the high bandwidth and slew-rate provides stability to the system. The transimpedance amplifier converts the current through the electrodes into a voltage signal (V_{OUT}) by means of a sensing resistor (R_{SENSE} in Figure 18A). The AD8066 have a JFET input to attenuate the current losses through the input impedance, the main drawback of this configuration [16]:

$$Z_{CELL} = \left(\frac{V_{IN}}{I_{CELL}} \right)$$

$$V_{OUT} = -R_{SENSE}.I_{CELL} = -R_{SENSE} \left(\frac{V_{IN}}{Z_{CELL}} \right)$$

The RMS-to-DC converter is the AD8436 from Analog Devices (Norwood, MA, USA) that provides a DC equivalent (V_{RMS}) of the transimpedance amplifier AC signal (V_{OUT}). It is a low power consumption device with a ZFET input buffer for electronic isolation from the instrumentation stage. Considering the biasing voltage (V_{IN}) and the sensing resistor (R_{SENSE}) stable and well known, the variations of DC voltage V_{OUT} are only related to the variations of Z_{CELL}. The device output voltage (V_{RMS}) is inverse compared to the HCT values on the blood sample, so as the HCT increases, V_{RMS} decreases.

A software interface on an external computer, connected by means of a NI USB-6361 data acquisition (National Instruments, Dallas, TX, USA), controls an electric switch to enable the power supply providing the measurement, and presents the resultant data on a user-friendly user interface (Figure 18D).

However, one of the main advantages of the presented device is the readout stage versatility which is capable of addressing different applications (Figure 18C), such as an integrated LCD display for an untrained user self-screening, a remote computer connected by a standardized protocol (USB, ethernet, Bluetooth, etc.) for telemedicine applications. In addition, the presence of an electrical signal directly correlated to HCT, and the high level of integration, allows the device implementation as a controller of other clinical actuators in different environments and situations, increasing functionalities of other devices and applications.

The overall low-cost and low power consumption system composed of optimized straightforward standards for instrumentation electronics results in a reusable, robust, and low power consumption device (<300 mWh), making it completely mobile with a long battery life time.

4.3. Low-cost PoC anemia detection device validation

4.3.1. Blood samples

Twenty four whole blood samples were obtained in 4 mL tubes containing EDTA (7.2 mg; BD Vacutainer, Franklin Lakes, NJ, USA), from four random hospitalized patients in Hospital Clinic. The whole blood samples were centrifuged (Jouan CR412 from DJB Labcare, Newport Pagnell, UK) at 2200 rpm for 15 minutes to separate blood plasma from RBCs. To obtain 24 blood samples, RBCs were diluted in different volumes of blood plasma using an automatic pipette Labopette Manual 10–100 μL (Hirschmann Laborgeräte, Louisville, KY, USA). Blood plasma was used as a reference value. We performed a CBC of the 24 blood samples with an

http://dx.doi.org/10.5772/60843

ABX Micros 60 hematology analyzer (Horiba, Kyoto, Japan) which reported the hemoglobin and HCT results as g/dL and percentage (%), respectively.

4.3.2. PoC device validation

To validate the PoC device for instantaneous detection of anemia, we analyzed 24 consecutive blood samples from patients hospitalized at Hospital Clínic in Barcelona. We tested all samples with the prototype within 2 hours of blood collection and CBC. Every whole blood sample was tested five times consecutively using fresh sensors and fresh sub-samples. Figure 19 depicts the output DC voltage (V_{RMS}) of the device and compares it with the different whole blood samples HCT.

$$V_{RMS}\left(mV\right) = \alpha + \beta\,\mathrm{HCT}$$

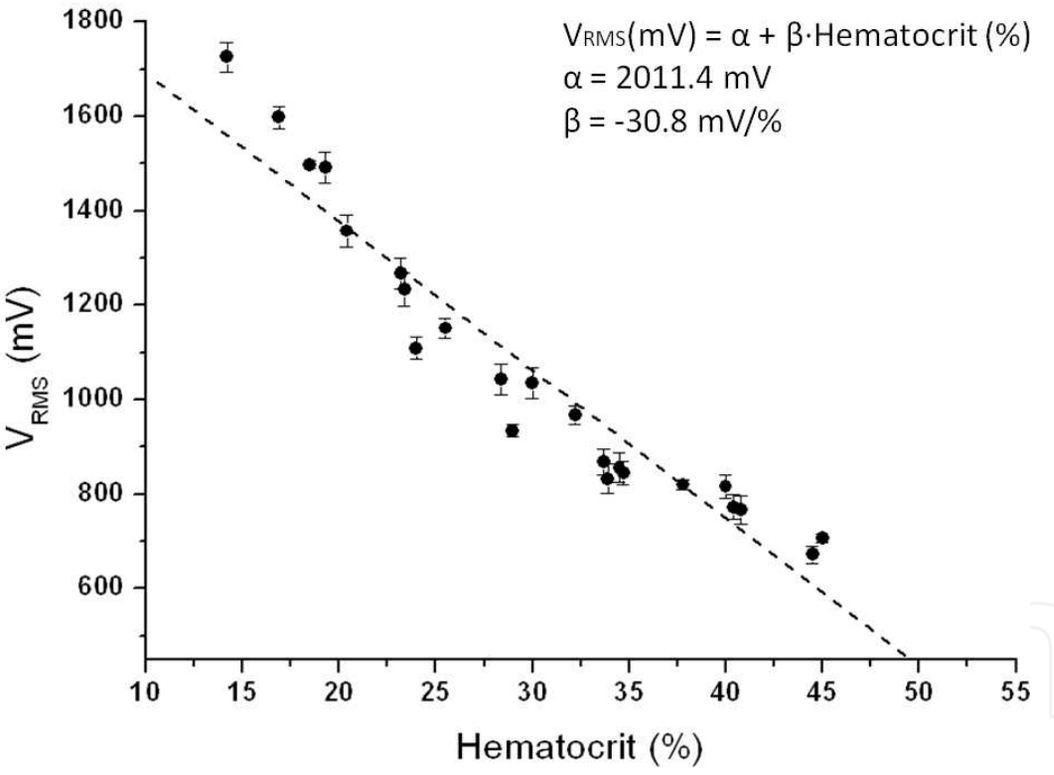

Figure 19. Measured output DC voltage (V_{RMS} (mV)) mean value (n = 5) as a function of blood samples HCT (HCT (%)).

The proposed anemia detector device presented a correlation coefficient of −0.96, an accuracy error of 2.83% HCT, and a coefficient of determination of 92.72%. The mean coefficient of variation is 2.57% without any particular case above 5%. This result represents a great performance and accuracy, according to the acceptable standards in quality control procedures in clinical hematology [50]. The device presents reliable, sensitive, and robust anemia detection compared with other commercial PoC devices, such as AnemiaCheck from Express Diagnos-

tics (Blue Earth, MN, USA), STAT-Site from Stanbio Laboratory (Boerne, TX, USA), or HemoPoint H2 from Alere (Waltham, MA, USA).

5. Conclusions

The PoC device outputs instantaneous reliable results based on electric voltage data directly correlated to HCT. The system has further versatility in terms of applications, compared with other commercial devices, due to the stable DC voltage output. It is an interesting tool as a PoC HCT detector for non-skilled users, a monitoring device for telemedicine patient monitoring, and can be used as a controller of other clinical actuators on more complex lab-on-a-chip devices. Furthermore, one of the most important features of an impedance-based device is that, unlike actual clinical equipment for blood analysis, RBCs are not destroyed in the measurement process, mitigating the adverse effects for patients and samples. Actual commercial devices for PoC anemia detection, based on microfluidic manipulator devices, such as AnemiaCheck from Express Diagnostics (Blue Earth, MN, USA), STAT-Site from Stanbio Laboratory (Boerne, TX, USA), or HemoPoint H2 from Alere (Waltham, MA, USA), rely on slower hemoglobin measurement for a subsequent HCT indirect calculation, with results open to ambiguous readout stages optically interpreted, and decrease functionalities and versatility, with a similar detection performance compared to the proposed PoC device (Table 3).

In summary, this chapter describes the design, development, and test of a PoC anemia detection device with low-cost disposable sensors and specific electronics, highlighting the different advantages and drawbacks of PoC electronic devices for biomedical applications.

Device	Test Time (sec.)	Range (HCT (%) and Hb (g/dL))	Standard Deviation (%)	Coefficient Variation (%)
Presented device.	Instantaneous	HCT: 0%–100%	2.83%	2.57%
STAT-Site (Stanbio Laboratory, Boerne, Texas).	900	HCT: 12%–42%	0.74%	4.10%
HemoPoint H2 System (Alere, Waltham, Massachusetts).	120	Hb: 5.6 g/dL–20.6 g/dL	NA	4.20%
Anemia Check (Express Diagnostics, Blue Earth, Minnesota).	60	Hb: 0 g/dL–25.6 g/dL HCT: 36%–54%	NA	1.5%
Tybursky et al. [52]	60	Hb: < 9 g/dL–"/> 12 g/dL	NA	NA

Table 3. Comparison of Point-of-care devices for HCT and Hb detection.

Author details

Jaime Punter-Villagrasa[1*], Joan Cid[2], Jordi Colomer-Farrarons[1], Ivón Rodríguez-Villarreal[3] and Pere Ll. Miribel-Català[1]

*Address all correspondence to: jpunter@el.ub.es

1 Department of Electronics, University of Barcelona, Barcelona, Spain

2 Department of Hemotherapy and Hemostasis, CDB, IDIBAPS, Hospital Clínic, Villarroel, Barcelona, Spain

3 Centre de Recerca Matemàtica, Campus Bellaterra, UAB, Edifici C, Barcelona, Spain

References

[1] N. Ramirez, A. Regueiro, O. Arias and R. Contreras, "Electrochemical impedance spectroscopy: An effective tool for a fast microbiological diagnosis," Biotecnologia Aplicada, vol. 26, pp. 72–78, 2008.

[2] G.A. Pop, L.L. Bisschops, B. Iliev, et al., "On-line blood viscosity monitoring in vivo with a central venous catheter, using electrical impedance technique," Biosens Bioelectron, vol. 41, pp. 595–601, March 2013.

[3] G.A. Pop, W.J. Hop, M. van der Jagt, et al., "Blood electrical impedance closely matches whole blood viscosity as parameter of hemorheology and inflammation," Appl Rheol, vol. 13 (6), pp. 305–312, 2003.

[4] F. Hernández, C. Guerrero and J. Bernal, "Determinación de las propiedades eléctricas en tejido sangíneo," Ciencia UANL, 8 (4), April 2011.

[5] R. Pradhan, A. Mitra and S. Das, "Impedimetric characterization of human blood using three-electrode based ECIS devices," J Electr Bioimpedance, vol. 3, pp. 12–19, January 2012.

[6] B. Ramaswamy, T.Y. Yin-Ting and Z. Si-Yang, "Microfluidic device and system for point-of-care blood coagulation measurement based on electrical impedance sensing," Sensors Actuators B: Chem, vol. 180, pp. 21–27, April 2013.

[7] N. Ramirez, A. Regueiro, O. Arias and R. Contreras, "Electrochemical impedance spectroscopy: An effective tool for a fast microbiological diagnosis" Biotecnologia Aplicada, vol. 26, pp. 72–78, 2009.

[8] N. Li, A. Brahmendra, A.J. Veloso, et al., "Disposable immunochips for the detection of Legionella pneumophila using electrochemical impedance spectroscopy," Anal Chem, vol. 84, pp. 3485–3488, March 2012.

[9] M. Dweik, R.C. Stringer, S.G. Dastider, et al., "Specific and targeted detection of viable Escherichia coli O157:H7 using a sensitive and reusable impedance biosensor with dose and time response studies,"Talanta, vol. 94, pp. 84–89, 2012.

[10] M. Grossi, M. Lanzoni, A. Pompei, et al., "An embedded portable biosensor system for bacterial concentration detection," Biosens Bioelectron, vol. 26, pp. 983–990, 2010.

[11] V. Lvovich, S. Srikanthan and R.L. Silverstein, "A novel broadband impedance method for detection of cell-derived microparticles," Biosens Bioelectron, vol. 26 (2), pp. 444–451, October 2010.

[12] M. Xu, X. Luo and J.J. Davis, "The label free picomolar detection of insulin in blood serum," Biosens Bioelectron, vol. 39, pp. 21–25, January 2013.

[13] R. Patterson, "Bioelectric Impedance Measurements: The Biomedical Engineering Handbook," J.D. Bronzino (ed.), 2nd edition. Boca Raton: CRC Press, pp. 734–73, 2000.

[14] C. Grosse and H.P. Schwan, "Cellular membrane potentials induced by alternating fields," Biophys J, vol. 63, pp. 1632–1642, 1992.

[15] B. Lenaerts and R. Puers, "Omnidirectional Inductive Powering for Biomedical Implants," Netherlands: Springer, 2009.

[16] J. Punter-Villagrasa, J. Colomer-Farrarons and P. Ll. Miribel, "Bioelectronics for Amperometric Biosensors, State of the Art in Biosensors: General Aspects." Dr. Toonika Rinken (ed.), 1st edition. Rijeka, Croatia: Intech, 2013.

[17] S. Park, J. Yoo, B. Chang and E. Ahn, "Novel instrumentation in electrochemical impedance spectroscopy and a full description of an electrochemical system," J Pure App Chem, vol. 5, pp. 1069–1080, August 2005.

[18] G. Li, M. Zhou, F. He and L. Lin, "A novel algorithm combining oversampling and digital lock-in amplifier of high speed and precision," Rev Sci Instrum, vol. 82, 095106, 2011.

[19] M.S. Cheng, J.S. Ho, S.H. Lau, V.T.K. Chow, and C.S. Toh, "Impedimetric microbial sensor for real-time monitoring of phage infection of Escherichia coli," Biosens Bioelectron, vol. 47, pp. 340–344, 2013.

[20] L. Yang, "Electrical impedance spectroscopy for detection of bacterial cells in suspensions using interdigitated microelectrodes,"Talanta, vol. 74, pp. 1621–1629, 2008.

[21] M. Min, O. Märtens and T. Parve, "Lock-in measurement of bio-impedance variations," J Int Measuret Confeder, vol. 27 (1), pp. 21–28, 2000.

[22] M. Gabal, N. Medrano, B. Calvo, et al., "A single supply analog phase sensitive detection amplifier for embedded applications," Proceedings of 25th Conference on Design of Circuits and Integrated Systems, DCIS2010, 17-19 November 2010, Lanzarote, Spain.

[23] C. Azzolini, A. Magnanini, M. Tonelli, G. Chiorboli and C. Morandi "A CMOS vector lock-in amplifier for sensor applications," Microelectron J, vol. 41 (8), pp. 449–457, 2010.

[24] C. Ribaut, K. Reybier, O. Reynes, et al., "Electrochemical impedance spectroscopy to study physiological changes affecting the red blood cell after invasion by malaria parasites," Biosens Bioelectron, vol. 24 (8), pp. 2721–2725, April 2009.

[25] R. Buendia, F. Seoane and R. Gil-Pita, "A Novel Approach for Removing the Hook Effect Artefact from Electrical Bioimpedance Spectroscopy Measurements," Journal of Physics, Conference on Electrical Bioimpedance, ICEBI2010, 4-8 April 2010, Gainesville, Florida.

[26] V.R. Taliene, T. Ruzgas, V. Razumas and J. Kulys, "Chronoamperometric and cyclic voltammetric study of carbon paste electrodes using ferricyanide and ferrocenemonocarboxylic acid," J Electroanal Chem, vol. 372, pp. 85–89, 1994.

[27] C. Beriet and D. Pletcher, "A microelectrode study of the mechanism and kinetics of the ferro/ferricyanide couple in aqueous media: The influence of the electrolyte and its concentration," J Electroanal Chem, vol. 361, pp. 93–101, 1993.

[28] S. Petrovic, "Cyclic voltammetry of hexachloroiridate(IV): An alternative to the electrochemical study of the ferricyanide ion," J Chem Educ, vol. 5 (5), pp. 231–235, 2000.

[29] C.A. Northrop-Clewes and D.I. Thurnham, "Biomarkers for the differentiation of anemia and their clinical usefulness," J Blood Med, vol. 4, pp. 11–22, March 2013.

[30] B. de Benoist, E. McLean, I. Egli and M.E. Cogswell, "Worldwide Prevalence of Anaemia 1993–2005: WHO Global Database on Anaemia" Geneva, Switzerland, 2008.

[31] World Health Organization, "Iron Deficiency Anaemia: Assessment, Prevention and Control: A Guide for Programme Managers," Geneva, Switzerland, 2001.

[32] N. Thakur, J. Chandra, H. Pemde and V. Singh, "Anemia in severe acute malnutrition," Nutrition. vol. 30, pp. 440-442, 2014.

[33] M. Rottoli, T. Sabharwal, A.M. Schizas and M.L. George, "Bleeding pseudoaneurysm of the internal iliac artery after extended resection for advanced rectal cancer: Report of two cases," Int J Colorectal Dis, 2014. DOI: 10.1007/s0038401419534.

[34] B. Ong and D.C. Rockey, "The syndrome of a large drop in hematocrit in hospitalized patients: Clinical features and gastrointestinal bleeding outcomes," J Investig Med, 2014. DOI: 10.1097/JIM.0000000000000109.

[35] National Heart, Lung, and Blood Institute, "What Is Sickle Cell Anemia?" Available at http://www.nhlbi.nih.gov/health/health-topics/topics/sca/ (accessed November 10, 2014).

[36] Medline Plus, "Thalassemia," Available at http://www.nlm.nih.gov/medlineplus/ency/article/000587.htm (accessed November 10, 2014).

[37] American Cancer Society, "Anemia in People With Cancer," Available at http://www.cancer.org/treatment/treatmentsandsideeffects/physicalsideeffects/anemia/anemia-in-people-with-cancer (accessed November 10, 2014).

[38] J. Portolés, J.L. Gorriz, E. Rubio, et al., "The development of anemia is associated to poor prognosis in NKF/KDOQI stage 3 chronic kidney disease," BMC Nephrol, 2013, 14, doi:10.1186/1471-2369-14-2.

[39] M. Pinto, M.L. Barjas-Castro, S. Nascimento, et al., "The new noninvasive occlusion spectroscopy hemoglobin measurement method: A reliable and easy anemia screening test for blood donors," Transfusion, vol. 53, pp. 766–769, April 2013.

[40] A. Belardinelli, M. Benni, P.L. Tazzari and P. Pagliari, "Noninvasive methods for haemoglobin screening in prospective blood donrs," Vox Sang, vol.105, pp. 116–120, April 2013.

[41] R.B. Thompson, "A Short Textbook of Haematology," fourth edition. Kent, England: Pitman Medical Publishing Co, 1975.

[42] D.J. Ernst, L.O. Ballance, R.R. Calam, et al., "Procedures and Devices for the Collection of Diagnostic Capillary Blood Specimens: Approved Standard," sixth edition. Wayne, Pennsylvania: CLSI, 2008.

[43] S.D. Asha, A.C.F. Chan, E. Walter, et al., "Impact from point-of-care devices on emergency department patient processing times compared with central laboratory testing of blood samples: a randomised controlled trial and cost-effectiveness analysis," Emerg Med J, vol. 31,pp. 714–719, September 2014.

[44] C.D.H. Jones, J. Howick, N.W. Roberts, et al., "Primary care clinicians' attitudes towards point-of-care blood testing: A systematic review of qualitative studies," BMC Fam Pract, vol. 14, pp. 117, August 2013.

[45] P. Thavendiranathan, A. Bagai, A. Ebidia, A.S. Detsky and N.K. Choudhry, "Do blood tests cause anemia in hospitalized patients? The effect of diagnostic phlebotomy on hemoglobin and hematocrit levels," J Gen Intern Med, vol. 20, pp. 520–524, June 2005.

[46] Y. Zheng, E. Shojaei-Baghini, A. Azad, C. Wang and Y. Sun, "High-throughput biophysical measurement of human red blood cells," Lab Chip, vol. 12, pp. 2560–2567, July 2012.

[47] J.P. Esquivel, J. Colomer-Farrarons, M. Castellarnau, at al., "Fuel cell-powered microfluidic platform for lab-on-a-chip applications: Integration into an autonomous amperometric sensing device," Lab Chip, vol. 12, pp. 4232–4235, November 2012.

[48] R. Patterson, "Bioelectric Impedance Measurements" in The Biomedical Engineering Handbook, J.D. Bronzino (ed.), 2nd edition. Boca Raton: CRC Press, 2000, pp. 734–773.

[49] D.W. Hill and F.D. Thompson, "The effect of haematocrit on the resistivity of human blood at 37ºC and 100 kHz," J Med Bioll Eng, vol. 13, pp. 182–186, March 1975.

[50] L. Corash, "Laboratory Hematology: Methods for the Analysis of Blood," in Blood, Principles and Practice of Hematology, R.I. Handin, S.E. Lux and T.P. Stossel, (eds.), 1st edition. Philadelphia: JB Lippincott & Co, 1995, chap. 2, pp. 23–61.

[51] E.A. Tyburski, S.E. Gillespie, W.A. Stoy, et al., "Disposable platform provides visual and color-based point-of-care anemia self-testing," J Clin Invest, vol. 124, pp. 4387–4394, 2014.

IntechOpen